IOP Publishing Measurement Science and Technology

Meas. Sci. Technol. **24** (2013) 085601 (12pp) doi:10.1088/0957-0233/24/8/085601

Protocols for the high temperature measurement of the Seebeck coefficient in thermoelectric materials

Joshua Martin

Material Measurement Laboratory, National Institute of Standards and Technology, Gaithersburg, MD 20899, USA

E-mail: joshua.martin@nist.gov

Received 30 January 2013, in final form 10 April 2013
Published 2 July 2013
Online at stacks.iop.org/MST/24/085601

Abstract

In Seebeck coefficient metrology, the present diversity in apparatus design, acquisition methodology and contact geometry has resulted in conflicting materials data that complicate the interlaboratory confirmation of reported high efficiency thermoelectric materials. To elucidate the influence of these factors in the measurement of the Seebeck coefficient at high temperature and to identify optimal metrology protocols, we measure the Seebeck coefficient as a function of contact geometry under both steady-state and transient thermal conditions of the differential method, using a custom developed apparatus capable of *in situ* comparative measurement. The thermal gradient formation and data acquisition methodology, under ideal conditions, have little effect on the measured Seebeck coefficient value. However, the off-axis 4-probe contact geometry, as compared to the 2-probe, results in a greater local temperature measurement error that increases with temperature. For surface temperature measurement, the dominant thermal errors arise from a parasitic heat flux that is dependent on the temperature difference between the sample and the external thermal environment, and on the various thermal resistances. Due to higher macroconstriction and contact resistance in the 4-probe arrangement, the measurement of surface temperature for this contact geometry exhibits greater error, thereby overestimating the Seebeck coefficient.

Keywords: Seebeck coefficient, thermoelectric, metrology

(Some figures may appear in colour only in the online journal)

Introduction

The Seebeck coefficient is the constant of proportionality that quantifies the thermoelectric conversion of an applied temperature difference into an electric potential. Materials that exhibit large absolute Seebeck coefficients ($S \approx 100$–$200\ \mu V\ K^{-1}$ at their target operation temperature), in addition to other optimal transport properties, are considered candidates for use in thermoelectric applications [1–5]. These applications include automotive engine waste heat recovery, remote power generation, integrated circuit cooling, and solid-state refrigeration. Due to its intrinsic sensitivity to the electronic structure, the Seebeck coefficient is an essential physical parameter that is routinely measured to identify the potential thermoelectric performance of a material.

The diversity in apparatus design, data acquisition methodology, and contact geometry, has resulted in conflicting materials data that complicate the meaningful interlaboratory comparison of data [6–11]. To elucidate the influence of these factors in the measurement of the Seebeck coefficient at high temperature and to identify standard testing protocols, we measure the Seebeck coefficient as a function of contact geometry under both steady-state and transient thermal conditions of the differential method. The measurement of surface temperature by direct contact is not trivial, as thermal offsets are ubiquitous. Therefore, each system's unique contact interfaces, between the external environment, the probe, and

the sample, each with distinct thermal properties, engenders a parasitic thermal transfer with the local environment that perturbs the actual measured surface temperature. Following an overview of Seebeck coefficient measurement techniques, we detail the influence of interstitial media, including low pressure gases and graphitic foil, on the thermal contact resistance and thereby the measured Seebeck coefficient. Next, we discuss the influence of data acquisition methods. Finally, we report the measurement of the Seebeck coefficient as a function of probe arrangement under both steady-state and quasi-steady-state thermal conditions at high temperature.

Seebeck coefficient metrology

Measurement of the relative Seebeck coefficient, especially at high temperature (>300 K) where thermocouples are common, requires a minimum of three voltage measurements: one for the thermoelectric voltage ΔV and one each for the hot and cold thermocouple voltage for T_2 and T_1, respectively, that determine the temperature difference ΔT. Acquisition protocols for these parameters must adhere to the following criteria, defined previously [6] as (1) the measurement of the voltage and temperature at the same locations and at the same time; (2) contact interfaces with the sample that are Ohmic and isothermal; and (3) the acquisition of small voltages with minimal extraneous contributions. Under these conditions, the electric potential emergent under an applied thermal gradient is given by [6]:

$$V_{ab}(T_1, T_2) = \int_{T_1}^{T_2} S_{ab}(T)\,\mathrm{d}T = \int_{T_1}^{T_2} [S_b(T) - S_a(T)]\,\mathrm{d}T, \quad (1)$$

where $S_a(T)$ is the absolute Seebeck coefficient of the sample being measured and $S_b(T)$ is the known Seebeck coefficient of the reference wires. It is assumed that materials a and b are chemically and physically homogeneous and isotropic, such that V_{ab} is a function of (T_1, T_2) and is independent of the temperature distribution between the interfaces [12]. According to this definition, the measured Seebeck coefficient S_{ab} is explicitly relative and requires the correction $S_{ab} = S_b - S_a$, where S_b is the contribution of the second conductor, to obtain S_a, the Seebeck coefficient of the sample (hereafter referred to as S). In n-type (p-type) semiconductors the electric potential establishes in the opposite direction (same direction) of the thermal gradient resulting in a negative (positive) Seebeck coefficient. This convention ensures agreement between the Seebeck coefficient and the sign of the charge carriers.

There are two techniques used to measure the relative Seebeck coefficient: the integral and the differential. In the integral technique (or large ΔT), one end of the specimen is maintained at a fixed temperature T_1 while the opposite end is varied through the temperature range of interest, $T_2 = T_1 + \Delta T$ [6]. An analytic approximation is applied to the entire data set $V_{ab}(T_1, T_2)$, then differentiated with respect to T_2. The integral method approximates thermoelectric device operating conditions and can often minimize the influence of voltage offsets due to the large temperature differences and subsequently larger voltage signals. However, it is difficult to maintain a constant T_1 throughout the large ΔT at high temperatures, requiring additional corrections. It is therefore most useful for longer samples, wires, metallic ribbons, and semimetals.

In the more preferred differential method, a small thermal gradient ΔT is applied to the sample at an average temperature of interest $T_o = (T_1 + T_2)/2$, where $T_1 = T_o - \Delta T/2$, and $T_2 = T_o + \Delta T/2$. By expanding the Seebeck coefficient $S_{ab}(T)$ in a Taylor series with center T_o and integrating, equation (1) becomes

$$\frac{\Delta V_{ab}}{\Delta T} = S_{ab}(T_o) + \sum_{n=1}^{\infty} \frac{1}{(2n+1)!} \frac{\mathrm{d}^{2n} S_{ab}(T)}{\mathrm{d}T_0^{(2n)}} \left(\frac{\Delta T}{2}\right)^{2n} = S_{ab}(T_o) + \Delta S_{ab}(T_o). \quad (2)$$

The Seebeck coefficient can then be obtained by the ratio of the electric potential and the temperature difference: $S = \Delta V/\Delta T$, where ΔV is the electric potential, and $\Delta T = T_2 - T_1$ is the applied temperature difference, provided $\Delta T/T_o \ll 1$, and $\Delta S/S \ll 1$, when $V \propto T_o$ and the latter term in equation (2) can be neglected. Differential methods can be categorized into three conditions according to the behavior of the thermal gradient: steady-state (DC), quasi-steady-state (qDC), and transient (AC), with respect to the *observation* time scale, i.e., the time interval required to measure one voltage channel. Under steady-state conditions, the Seebeck coefficient is often calculated from the linear fit of multiple electric potential/temperature difference data points to avoid the assumption that the experimental data are collinear with the ordinate ($V = 0$, $\Delta T = 0$), effectively eliminating extraneous voltage offsets (≈1–100 μV). Thermal offsets cannot be eliminated using this technique. To overcome the time burden required to stabilize multiple steady-state ΔTs, the qDC condition employs an increasing heat flux where the voltage and temperature difference are continuously recorded.

In addition to these thermal conditions of the differential method, there exist two primary contact geometries (or probe arrangements). In the axial-flow arrangement (2-probe), the temperature difference and the electric potential are measured *on the probes* which are in direct contact with the ends of the sample. This is the arrangement preferred by Goldsmid and Tritt for improved thermal and electrical contact [9]. However, many Seebeck coefficient apparatus also concurrently measure resistivity, requiring additional voltage contacts away from the ends of the sample. In the potentiometric arrangement (or 4-probe), the temperature difference and the electric potential are measured between two locations *on the sample* (or inserted within the sample) equidistant from the hot and cold probes.

There is little comparative research to substantiate which contact geometry, if any, provides the more accurate determination of temperature and voltage. In 1959, Bowers [13] compared the Seebeck coefficient as measured using chromel–alumel thermocouples, inserted within nickel probes pressed at the ends of the sample for the 2-probe geometry, and inserted within 0.8 mm holes drilled halfway within the sample for the 4-probe geometry. The absolute Seebeck coefficients measured using the 4-probe arrangement were ≈ 10% larger

than those obtained using the 2-probe arrangement up to 500 °C. There was considerable scatter in the data obtained using the 4-probe arrangement and data obtained using the 2-probe arrangement above 500 °C were corrected for better agreement but no further details on that procedure were provided. In addition, there was no estimation made of the overall measurement uncertainty so comparison of the two geometries is challenging. Wood [14] also compared the results obtained by using niobium–tungsten thermocouples pressed on the ends of a sample with those obtained by inserting the same type of thermocouple in holes drilled into the sample. The results were consistent within the measurement uncertainty; however, data for only one temperature were included and the actual temperature was not specified. Finally, neither of these reports measured the Seebeck coefficient using surface contact temperature probes, a prevalent design of modern thermoelectric apparatus.

Instrumentation

Measurements were conducted in a custom developed apparatus capable of *in situ* evaluation and comparison of the Seebeck coefficient as measured under multiple thermal conditions and surface-mounted probe arrangements. The salient features are restated below for completeness. Reference [15] describes the primary components in more detail.

The local temperature is maintained using a 7.2 kW ULVAC RHL-P65C tube furnace[1], consisting of a concentric series of six infrared emitting tungsten elements, each mounted at the focal point of a parabolic gold reflector. This geometry provides axial and radial thermal profiles that are temporally and spatially consistent. The furnace temperature is monitored through a custom spark welded 0.125 mm Pt–Pt + 13% Rh bare wire thermocouple mounted in an extruded alumina twin bore tube and wrapped in a molybdenum radiation shield. Once the setpoint has stabilized, the thermal oscillations as observed from the furnace thermocouple are below 50 mK throughout the stated temperature range.

The furnace encloses a 100 mm DIA (diameter) single ended quartz tube that mates to the vacuum chamber through a series of water cooled O-ring connecting flanges. The sample probe is centered within this quartz tube and supported through an opening in the vacuum chamber. To maintain an inert and contaminant free environment, the sample chamber is evacuated below 10^{-2} Pa (10^{-4} Torr) using a magnetic bearing Pfeiffer TMH 071P turbomolecular drag pump, roughed in line by an oil-free Pfeiffer MVP 015 diaphragm pump.

The sample probe is uniquely machined with relief features to accommodate multiple sample configurations, including parallelepiped (2–18 mm height) and disc geometries (6.35 mm radius), both in transverse and longitudinal orientation. In addition, the probe design enables measurement of the Seebeck coefficient in both 2- and 4-probe arrangements. This allows for routine comparison of both arrangements and expands the practical range of sample size and geometry. For the 2-probe arrangement, thermocouples are spark welded to the upper and lower electrodes and encapsulated within an aluminum nitride (AIN) coating; 4-probe measurements are accomplished by means of two small diameter thermocouples pressed onto the sample between the top and bottom probes used in the 2-probe arrangement. The upper and lower probes are inverse configurations.

Tungsten was selected for the electrode probe material due to its low electrical resistivity (52.8 nΩ m), high thermal conductivity (174 $\mathrm{W\,m^{-1}\,K^{-1}}$) and desirable physical properties. Each tungsten electrode (19.05 mm DIA) features a corresponding raised alignment notch to enable straightforward sample mounting (centered for a 2.5 mm × 2.5 mm cross section area sample and perpendicular to the 4-probe thermocouples) and to maintain a consistent furnace immersion depth for the 4-probe thermocouples that press onto the sample. In this way, any chemical inhomogeneity signature that develops in the thermocouples as a function of thermal profiles will remain consistent between measurements.

Each tungsten electrode is precisely fitted within electrically insulating support sleeves. These are fabricated from AlN ceramic cylinders (25.4 mm DIA × 28.58 mm tall) and bonded to the tungsten using AlN-based adhesive (Aremco 865C). AlN has a high thermal conductivity ≈180 $\mathrm{W\,m^{-1}\,K^{-1}}$ with an average thermal expansion coefficient identical to tungsten. Controlled thermal gradients for Seebeck coefficient measurements are formed by passing current through either of two heater coils, each bonded to the upper and lower AIN probe sleeves using a thin layer of AIN adhesive. These coils are comprised of custom bifilar wound (non-inductive) tungsten–rhenium alloy wires electrophoretically coated with alumina for electrical isolation. Bipolar heating allows for zero-gradient resistivity measurements as well as toggled Seebeck coefficient measurements to conduct thermal offset checks.

The probe assembly features simultaneous multi-axis movement for adjustment to the upper and lower probe distance (for variation in sample height), and for movement of the 4-probe thermocouples to and from the sample. A magnetic spring-balanced, linear bearing assembly performs automatic adjustment of the 4-probe thermocouples' vertical spacing in a continuum, optimally selected for various sample heights. The ratio of the probe spacing to sample height is also adjustable. Vertical movement of both the upper and lower probes and the 4-probe thermocouples is accomplished using a twin lead screw slider for dual opposing motion connected. The upper and lower SIALON tubes are mounted to either of the two coaxial dovetail slider mounts. A NEMA 23, 1.8° bipolar step motor with a resolution up to 1/256 step is used to adjust the twin slider positions, where the pressing force is modulated by adjusting the motor current and velocity (along the torque curve). The 4-probe thermocouple alumina tubes are mounted external to the furnace using independent sliders fitted with compression springs ($k = 1.91$) to maintain the pressure of the thermocouple interface. These sliders are mated through

[1] Certain commercial equipment, instruments, or materials are identified in this document. Such identification does not imply recommendation or endorsement by the National Institute of Standards and Technology, nor does it imply that the products identified are necessarily the best available for the purpose.

a series of vacuum compatible linear bearings to a rotary-to-linear vacuum feedthrough, also fitted with a bipolar step motor for horizontal positioning.

Temperature measurement for each of the 2- and 4-probe location pairs is accomplished using 0.125 mm Pt–Pt + 13% Rh thermocouples (Omega Engineering), with the entire length embedded in a twin bore alumina sheathing to avoid strain and contamination. This wire diameter can reduce parasitic heat sinking without significantly increasing contamination susceptibility or drift. Bentley [16] provides a thorough discussion of thermocouple theory, error reduction, and methods to estimate the total uncertainty. The thermocouples were cleaned with ethanol prior to assembly, then annealed together in air at 1100 °C in a tube furnace and cooled over 2 h to 300 °C [16, 17] to ensure calibration. A thermocouple that is not in calibration can contribute an additional error of 0.3 K [16]. The thermocouple tips are shielded from thermal radiation using two polished molybdenum radiation shields. One shield rests between the lower and upper probe to trace the temperature along the sample, while the second shield encloses the entire probe along the axis of the furnace. Individual thermal fluctuation for each thermocouple at 295 K is below 10 mK and the deviation between each thermocouple temperature is less than 60 mK [15]. The thermal stability is typically between 20 and 40 mK at higher temperatures. This is better than the overall furnace stability due to the thermal mass of the probe.

In this embodiment, measurement of the Seebeck coefficient is explicitly relative (equation (1)). The measured value is proportional to the difference between the Seebeck coefficient for the material of interest and that for the reference wires. Therefore the Seebeck coefficient of the reference material must be determined in a separate experiment throughout the temperature range of interest. The most accurate reference data have been obtained by Roberts for Pt between 273 and 1600 K by measuring the Thomson heat μ_T (or Thompson coefficient) directly [18]. Burkov [19] provides an empirical interpolation function for the Seebeck coefficient of Pt between 70 and 1500 K and estimates the uncertainty for this absolute thermoelectric scale as ± 0.1 μV K^{-1} at temperatures between 70 and 900 K, increasing to ± 0.5 μV K^{-1} at 1500 K.

Thermocouples provide a relative measurement of temperature that requires accurate knowledge of a reference temperature. Inaccurate measurement of this reference temperature increases the uncertainty in the measurement of a thermocouple temperature by ≈0.05 K [16]. The terminal block functions as the interface for each thermocouple lead wire to the voltage measurement device. The temperature of the interface between these thermocouple wires and the voltmeter is the reference temperature. To achieve uniform temperature distribution between all terminals with respect to this single reference temperature, a custom isothermal terminal block was constructed. This is composed of a high thermal conductivity AlN substrate with metalized surfaces, stack soldered to an oxygen free (OF) copper base plate on the bottom and to individual OF copper screw terminal blocks on the top. Complete design and assembly details are provided in [15]. The reference temperature is measured using a calibrated (NIST traceable) platinum resistor (Lake Shore Cryotronics, Inc. Model PT-103-AM-70H) soldered and screwed to the surface of the center copper terminal blocks to best represent the temperature at each contact location. The manufacturer's quoted measurement uncertainty at 295 K is 22 mK.

The series of connections between the thermocouple wires and the nanovoltmeters are formed using copper to copper pressure interfaces to minimize thermoelectric voltage offsets below 0.2 μV. All copper interfaces are polished and then cleaned prior to assembly using a Deoxit brand solution. The thermocouple voltage, thermoelectric voltage, resistance voltage, and platinum resistor voltage are all measured using three Keithley 2182A nanovoltmeters. At any given time, two of the meters are dedicated to the T_2 and T_1 thermocouples (2- or 4-probe) and the third is connected to an eight-channel 7168 nV scanner card inserted within a Keithley 7001 switch mainframe to scan between the thermoelectric voltage and other signals. The nanovolt scanner card does not degrade the noise and drift performance of the 2182A, nor does it increase the uncertainty. All nanovoltmeters are fitted within an air-cooled and temperature stable enclosure. The quoted uncertainty for the 2182A under optimal settings and during the standard calibration period is 40 nV (under a square distribution).

Type B uncertainties are systematic in origin and primarily derive from instrumentation, data acquisition, and/or calibration errors. Only those systematic uncertainties arising from the measurement of the hot and cold thermocouples and the electric potential are considered. At 295 K, the voltage reading for an R-type thermocouple is ≈ 10 μV and the standard uncertainty is 0.4%. In addition, the thermocouple manufacturer's quoted accuracy is 0.25 K. Therefore, the combined standard measurement uncertainty for each thermocouple is 0.48% T. The uncertainty in ΔT is $(0.48^2 + 0.48^2)^{1/2}\% = 0.68\%$. Consequently, the Seebeck coefficient, computed as the least square estimate of the slope based on the data $\{(\Delta T, \Delta V)\}$, at each temperature point T, has the same 0.68% uncertainty. There is also an uncertainty arising from the average sample temperature measurement, T, given by the compound average of the collection of sample temperature values obtained for each ΔT and ΔV pair, where each sample temperature is calculated as the simple average using the hot and cold thermometer measurements. The uncertainty for the average of two temperatures can be computed easily in terms of uncertainties for individual temperatures, i.e., $((0.48/2)^2 + (0.48/2)^2)^{1/2}\% = 0.34\%$. These are combined for a total uncertainty of 0.76%. The type B expanded uncertainty for the Seebeck coefficient is then $\pm 1.5\%$ (with a coverage factor $k = 2$ for a 95% confidence level).

Identifying error arising from nonisothermal contact

In this embodiment, the method of forming good electrical and thermal interfaces between the probes and the sample at

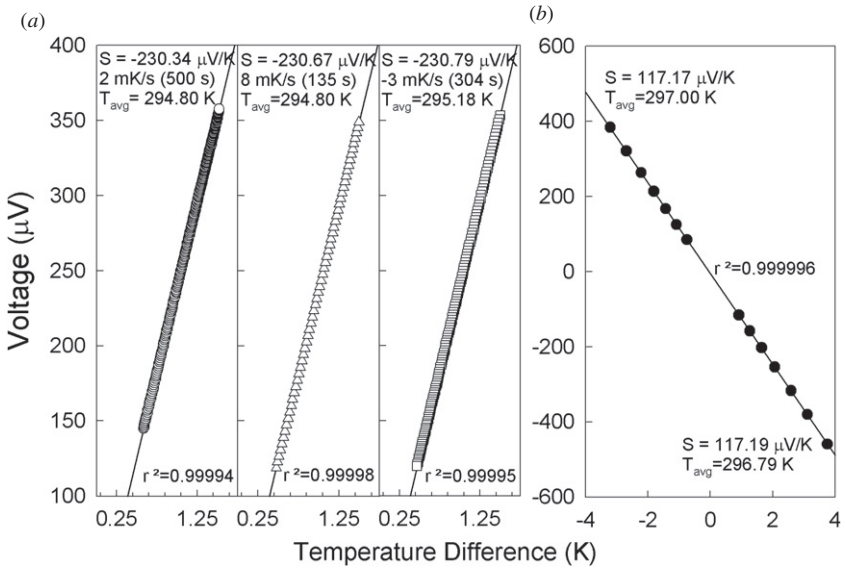

Figure 1. (*a*) Comparison of voltage versus temperature difference plots obtained under the qDC condition for three different heat pulses: 2, 8 and −3 mK s^{-1} with similar average sample temperatures T_{avg}. (*b*) Voltage versus temperature difference plot obtained under the DC condition for a positive and negative thermal flux.

high temperature is using pressure modulated surface contacts, since this temperature range limits the practical use of solders and epoxies. There are many references that describe the challenges of forming Ohmic contacts between metal and semiconductor interfaces [20, 21]. One diagnostic test is to conduct current–voltage (*IV*) sweeps at each measured temperature. In this apparatus, the linear regression typically approximates the I and V data better than 4σ (99.993%), indicating Ohmic behavior. The typical zero current–voltage offset is between 0.2 and 5 μV. Assuming the data are not collinear with the ordinate ($V = 0$, $\Delta T = 0$), these extraneous voltage offsets can be effectively eliminated by calculating the Seebeck coefficient from the linear fit of multiple electric potential/temperature difference data points.

However, thermal offsets are inherently ubiquitous and cannot be eliminated using this technique. The nature of each system's unique contact interfaces, between the external environment, the probe and the sample, each with distinct thermal properties, engenders a parasitic thermal transfer that perturbs the actual measured surface temperature. Therefore, the challenge of forming good thermal contacts cannot be overstated. Thermal interface quality can be evaluated by identifying the degree of hysteretic behavior. For example, under the quasi-steady-state condition, a discrepancy between the Seebeck coefficient measured under different heating rates may indicate a poor thermal contact. Figure 1(*a*) compares voltage versus temperature difference plots obtained on a Bi_2Te_3 sample (SRM 3451) under three different heat pulses: 2, 8 mK s^{-1}, and one inverted heat pulse, −3 mK s^{-1}. These data were recorded for a temperature difference between 0.5 and 1.5 K and for similar average sample temperatures (compound average). The linear regressions approximate the voltage and temperature difference data better than 4σ. The Seebeck coefficients for all three data sets agree within 0.5 μV K^{-1}, including the value obtained under a negative heat pulse. A similar diagnostic can be performed under the steady-state condition, by measuring the Seebeck coefficient with thermal gradients stabilized by heating from the bottom probe and with inverted gradients by heating from the top probe. Figure 1(*b*) plots a representative example of this diagnostic measured on a polycrystalline $Si_{80}Ge_{20}$ sample by stabilizing seven incremental ΔTs between 0.25 and 4 K and between –0.25 and –4 K. The Seebeck coefficient obtained for the positive thermal flux is 117.19 μV K^{-1} and is 117.17 μV K^{-1} for the negative thermal flux. The linear regression approximating both positive and negative voltage and temperature difference data sets is better than 4.5σ (99.9993%). The absence of thermal hysteresis in the Seebeck coefficient is one reliable indication of an isothermal contact interface. It is therefore prudent to perform these diagnostic tests periodically throughout the measurement cycle.

Low pressure gases are often introduced to enhance the thermal contact between the thermocouple and the sample. For example, many commercial apparatus require back filling of helium gas between 25 and 30 kPa (≈200 Torr) to achieve reliable thermal contact. There are reports suggesting low pressure gases such as helium and nitrogen may affect the measured Seebeck coefficient value [15, 22, 23]. The presence of high thermal conductivity gases will introduce additional parasitic heat losses and consequently error in the Seebeck coefficient. Without sufficient measurements on standardized reference materials, it is a challenge to select the optimal gas pressure. The evacuation of the sample chamber can significantly affect the Seebeck coefficient value for a material measured under a poor thermal contact. Figure 2 plots the Seebeck coefficient measured as a function of pressure for nitrogen (open squares) and for helium gas (open circles) measured in the 2-probe arrangement with a poor thermal contact under the qDC condition at 295 K. Data at the highest and lowest pressures were also confirmed by measuring under

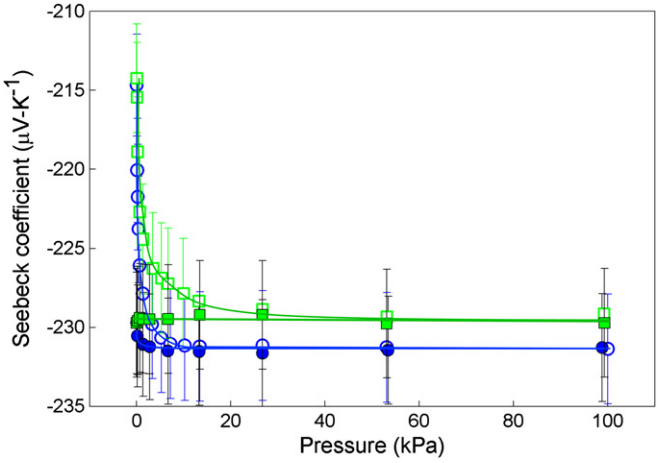

Figure 2. Seebeck coefficient as a function of helium (circles) and nitrogen (squares) gas pressure at 295 K for Bi_2Te_3 SRM 3451 measured under a poor thermal contact (unfilled circles) and the Seebeck coefficient using a graphite-based foil interface (filled circles). The error bars represent the ± 1.5 expanded uncertainty described in the text. The lines are a guide for the eye.

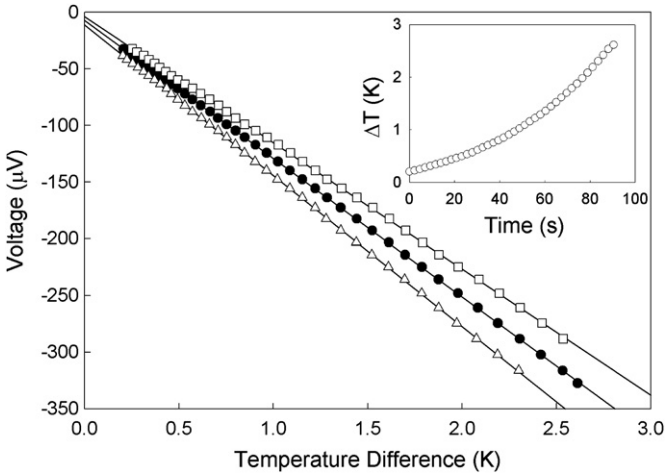

Figure 3. Experimental results of a Seebeck coefficient measurement on polycrystalline $Si_{80}Ge_{20}$ under simultaneous acquisition (filled circles), compared with the Seebeck coefficients under a 2.3 s staggered acquisition for a V:T_2:T_1 sequence (open squares) and the inverse T_1:T_2:V sequence (open triangles). The Seebeck coefficient for the simultaneous acquisition is 117.26 μV K^{-1}, compared with 106.53 μV K^{-1} (V:T_2:T_1) and 128.24 μV K^{-1} (T_1:T_2:V) representing a 9.5% error. The inset shows the nonlinear time dependence of the temperature difference.

the DC condition to preclude any influence of measurement technique. The data obtained under high vacuum are noticeably lower than those obtained under ambient pressure and to the reference value [24]. The standard deviation for all the average sample temperatures is 0.25 K. The Seebeck coefficient value normalizes above 25 kPa for nitrogen gas and above 5 kPa for helium gas, since helium has a comparatively large heat capacity and thermal conductivity. In addition, the absolute Seebeck coefficients measured under helium gas are marginally larger than those under nitrogen gas. This disparity may suggest a larger convective cooling of the thermocouples, and hence a surface temperature measurement error. However, the data measured at these higher pressures agree within the measurement uncertainty, so it is prudent to avoid broad conclusions.

A tacit assumption is that a linear voltage versus temperature difference plot is indicative of an isothermal contact. However, the linear relationship for these data ($r^2 = 0.999\,98$) suggest the better assumption is that while a nonlinear relationship may imply a poor thermal contact, a linear relationship does not imply a good thermal contact. Fortunately, the thermal contact can be modified using a thermal interface material. The closed symbols in figure 2 are the Seebeck coefficients for the same Bi_2Te_3 SRM material, measured in the 2-probe arrangement, but using graphitic interface foil between the sample and each tungsten probe to reduce the thermal contact resistance (Graftech International eGraf HT 1210). The data obtained under high vacuum are identical to those obtained under all pressures measured, including ambient conditions. This interface material is routinely used to enhance the thermal contact and does not increase the contact voltage offset as measured using *IV* sweeps. In addition, the foil creates a barrier to prevent chemical reaction of the test sample with the tungsten probes. Alternative diffusion barriers include nickel, tantalum or platinum thin foils.

Error arising from staggered acquisition

Some implementations using the quasi-steady-state condition incorporate only one voltmeter and a voltage channel switcher, and thereby stagger the acquisition of the ΔV, T_2 and T_1 parameters. As a result, the thermal drift between each parameter acquisition introduces error in the measured Seebeck coefficient by distorting the temperature–voltage correspondence. Consequently, the character of the distortion is dependent on the parameter acquisition sequence. In this embodiment, the three nanovoltmeters (two dedicated to the T_2 and T_1 thermocouples and the third to measure the thermoelectric voltage) simultaneously measure each parameter to avoid staggered acquisition errors. This is accomplished programmatically using a GPIB bus trigger.

One method to explore the effect of voltage/temperature correspondence distortion under the qDC condition is to program the three nanovoltmeters to simultaneously acquire the data, then combine the successive thermoelectric voltage and hot and cold thermocouple readings that model a specific time delay. In this manner, it is possible to mimic the acquisition that would occur using only one nanovoltmeter and a switching card but retain the data obtained by simultaneous acquisition. Since the data used are from one measurement cycle, this process ensures both the thermal heating rate and the average sample temperature are identical. The optimal accuracy for the 2182A nanovoltmeters is obtained for an NPLC (number of power line cycles) setting of 5. This corresponds to an aperture (analog to digital conversion) time of 83.3 ms and a total measurement time of ≈ 2.3 s (obtained experimentally). As a demonstration of staggered acquisition error, figure 3 shows the Seebeck coefficient measurement on a doped polycrystalline $Si_{80}Ge_{20}$ material under simultaneous

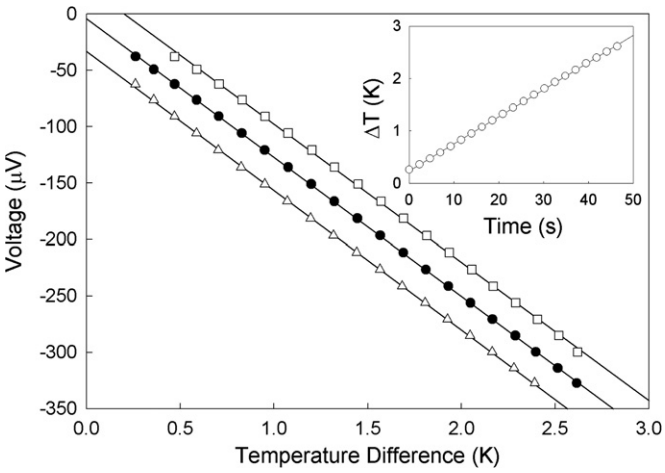

Figure 4. Experimental results of a Seebeck coefficient measurement on polycrystalline $Si_{80}Ge_{20}$ under simultaneous acquisition (filled circles), compared with the Seebeck coefficients under a 2.3 s staggered acquisition for a V:T_2:T_1 sequence (open squares) and the inverse T_1:T_2:V sequence (open triangles). The Seebeck coefficient for the simultaneous acquisition is 118.16 μV K^{-1}, compared with 117.72 μV K^{-1} (V:T_2:T_1) and 118.64 μV K^{-1} (T_1:T_2:V) representing only a 0.4% error. The inset shows the linear time dependence of the temperature difference.

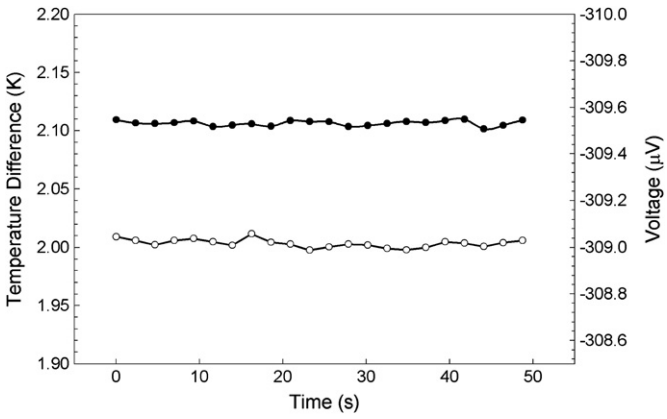

Figure 5. Representative plot depicting the temporal stability of the temperature difference (filled circles) and the voltage (unfilled circles) for a period of 60 s at 400 K.

acquisition (filled circles), compared with the Seebeck coefficients measured under a 2.3 s staggered acquisition for a V:T_2:T_1 sequence (open squares) and the inverse T_1:T_2:V sequence (open triangles). The Seebeck coefficient for the simultaneous acquisition is 117.26 μV K^{-1}, compared with 106.53 μV K^{-1} (V:T_2:T_1) and 128.24 μV K^{-1} (T_1:T_2:V). This represents a 9.5% error for a nonlinear average heating rate of 29 mK s^{-1}. Averaging the Seebeck coefficient obtained for one sequence and its inverse yields a value of 117.39 μV K^{-1}, similar to that obtained under simultaneous acquisition. This is also consistent with the error model developed to quantitatively explore the effect of temporal perturbation to the voltage and temperature correspondence using finite element analysis [25]. The error is proportional to the heating rate and the data acquisition delay. The error is also greater for a nonlinear heating rate than for a linear heating rate. Figure 4 shows the Seebeck coefficient measurement on the same polycrystalline $Si_{80}Ge_{20}$ material under simultaneous acquisition (filled circles), compared with the Seebeck coefficients measured under a 2.3 s staggered acquisition for a V:T_2:T_1 sequence (open squares) and the inverse T_1:T_2:V sequence (open triangles). The Seebeck coefficient for the simultaneous acquisition is 118.16 μV K^{-1}, compared with 117.72 μV K^{-1} (V:T_2:T_1) and 118.64 μV K^{-1} (T_1:T_2:V). This represents only a 0.4% error for a linear heating rate of 56 mK s^{-1}. Averaging the Seebeck coefficient obtained for one sequence and its inverse yields a value of 118.18 μV K^{-1}, similar to that obtained under simultaneous acquisition. An alternative solution to minimize the correspondence distortion error is to fit the time dependence of T_2 and T_1 and interpolate the values corresponding in time to the electric potentials. Therefore, errors arising from correspondence distortion can be minimized by instrumentation and/or software modification without requiring a complete apparatus redesign. If additional voltage measurement instrumentation are not available, the heating rate should be slow and progress linearly, with an increased data acquisition rate.

The Seebeck coefficient as a function of static and transient thermal conditions

To meaningfully compare the Seebeck coefficient as a function of steady-state and quasi-steady-state conditions of the differential method, all data were measured concurrently in the same thermal cycle. The Seebeck coefficients were measured on a p-type polycrystalline $Si_{80}Ge_{20}$ material between 300 and 900 K. The maximum sample temperature was 900 K to preclude dopant precipitation [26]. For measurements under the qDC condition, the maximum temperature difference was between $0.001T_o$ and $0.02T_o$ with gradient heating rates between 5 and 50 mK s^{-1}. Data were recorded simultaneously in 2.3 s intervals. The Seebeck coefficients were then obtained from the unconstrained linear fit of multiple electric potential/temperature difference data points. For measurements under the DC condition, six incremental temperature differences between $0.001T_o$ and $0.02T_o$ were allowed to stabilize for $\approx$ 30 min. The voltage and temperature differences were recorded for 60 s and averaged. The temporal stability of the temperature difference is typically within 10 mK and the voltage is within 100 nV. A representative plot is shown in figure 5 at 400 K. The Seebeck coefficients were then similarly obtained from the unconstrained linear fit of multiple electric potential/temperature difference data points. To ensure similar thermal conditions and avoid potential sample variability, the voltage and temperature difference data were measured for both 2- and 4-probe arrangements using the same stabilized gradients. Consequently, the temperature differences measured using the 2-probe arrangement were comparatively larger than those measured for the 4-probe. Since the linear regressions approximate the voltage and temperature difference data better than 4σ, and $\Delta S/S \ll 1$, the relative size of the temperature difference will have a negligible effect on the measured Seebeck coefficient value.

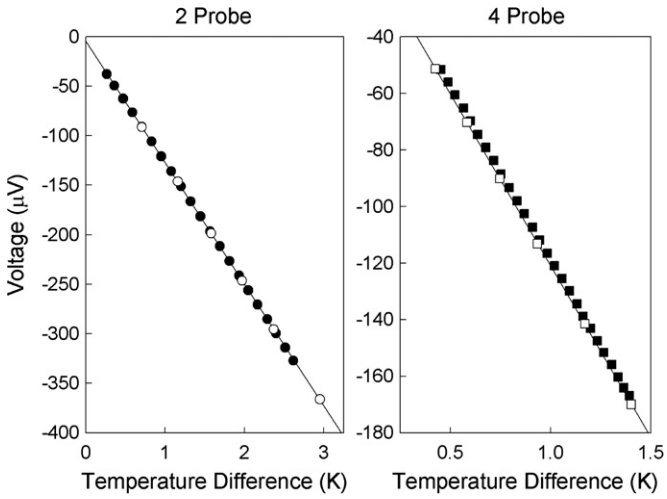

Figure 6. Room temperature voltage versus temperature difference plots for the 2-probe and 4-probe arrangements, each comparing data measured under both qDC and DC conditions. The obtained Seebeck coefficients agree within the measurement uncertainty.

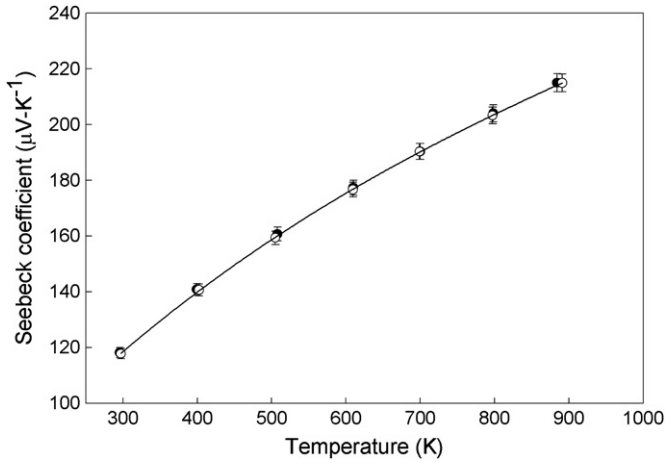

Figure 7. The temperature dependent Seebeck coefficient for $Si_{80}Ge_{20}$ measured under both qDC and DC conditions for the 2-probe arrangement. The error bars represent the ± 1.5 expanded uncertainty described in the text.

Figure 6 shows the room temperature voltage versus temperature difference plots for the 2-probe and 4-probe arrangements, each comparing data measured under both qDC and DC conditions. The obtained Seebeck coefficients agree within the measurement uncertainty. Figures 7 and 8 show the temperature dependent Seebeck coefficient, comparing data measured under both qDC and DC conditions for the 2-probe arrangement (figure 7) and for the 4-probe arrangement (figure 8). The Seebeck coefficients measured for each contact geometry agree within the measurement uncertainty, although the data measured using the DC technique are typically $\approx 0.5\ \mu V\ K^{-1}$ lower than the qDC data. These data indicate no dependence of the Seebeck coefficient on the measurement technique. Therefore, in the interest of measurement time, it should be acceptable to employ the qDC technique, provided

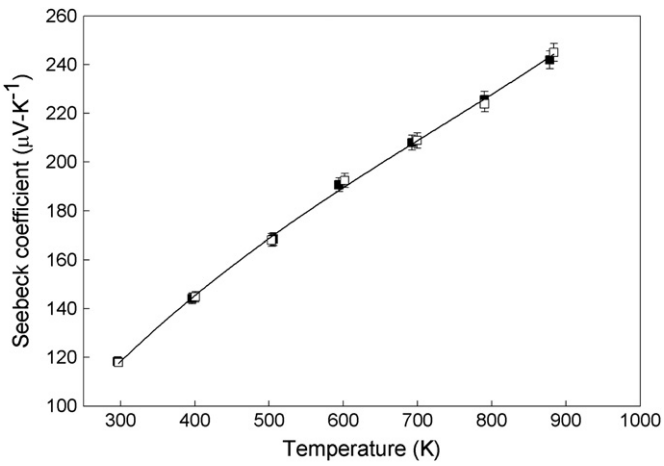

Figure 8. The temperature dependent Seebeck coefficient for $Si_{80}Ge_{20}$ measured under both qDC and DC conditions for the 4-probe arrangement. The error bars represent the ± 1.5 expanded uncertainty described in the text.

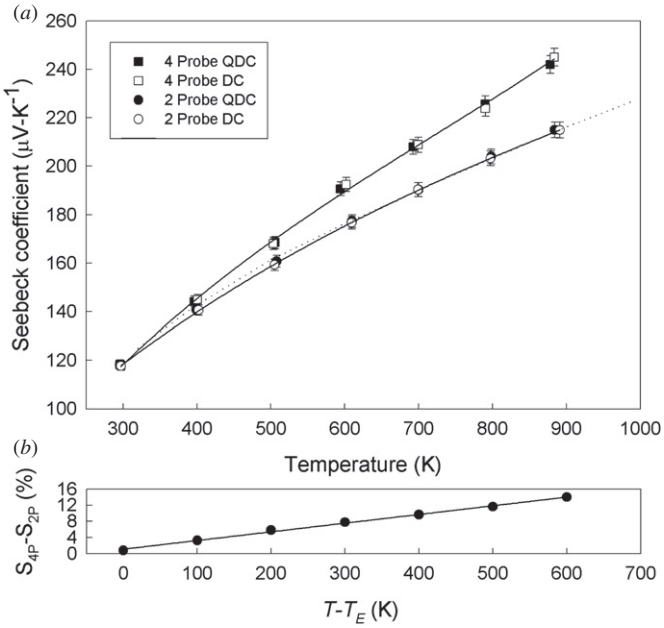

Figure 9. (*a*) The Seebeck coefficient measured as a function of contact geometry under both DC and qDC conditions. The data sets for the 2- and 4-probe arrangement diverge monotonically as the temperature increases. The dotted line is a fit to literature data extrapolated from [32]. (*b*) The divergence value is a linear function of the temperature difference between the sample and the external environment. The error bars represent the ± 1.5 expanded uncertainty described in the text.

the sensors are in very good thermal contact with the sample and the heating rate is slow.

The Seebeck coefficient as a function of contact geometry

Figure 9(*a*) compares the Seebeck coefficient measured as a function of contact geometry under both steady-state

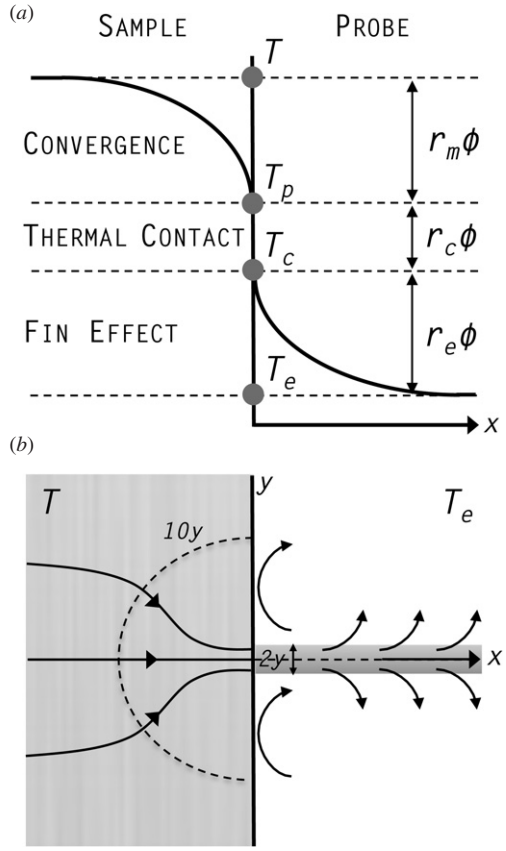

Figure 10. Steady-state error model for a homogenous semi-infinite sensor in non-perfect contact with a surface. (*a*) Diagram illustrating the thermal transfer as a function of distance *x*. (*b*) Physical illustration of the error model.

and transient thermal conditions. At room temperature, the Seebeck coefficients measured by the 2-probe arrangement and those measured by the 4-probe arrangement agree within the measurement uncertainty. However, the data sets diverge monotonically as the temperature increases. The divergence value is a linear function of the temperature, or more specifically, the temperature difference between the sample and the external environment (figure 9(*b*)). At 900 K, the difference between the 2-probe Seebeck coefficients and the 4-probe Seebeck coefficients approaches 14%. Data measured under the DC condition were obtained for both probe arrangements using the same stabilized temperature differences. However, the average sample temperatures obtained in the 4-probe arrangement, as compared to those obtained in the 2-probe arrangement, decrease with increasing temperature, reaching a difference of $\approx$ 0.9% at 900 K. The comparative differences in Seebeck coefficient can be understood in context of the error in measuring the surface temperature by contact.

The measurement of surface temperature by contact is influenced by intrinsic thermal errors. Application of a sensor to the surface of the medium modifies the superficial conductive, convective, and radiative interaction of the contacted surface with the environment, thereby inducing a parasitic thermal transfer between the sample and the sensor, and the sensor and the environment that perturbs the local temperature field. This error depends on the unique geometric and thermophysical characteristics of the system, requiring solutions of complex multidimensional heat transfer problems to develop an accurate corrective error model. It is sufficient for this discussion to consider a simplified error model and extract the relevant conceptual results.

The influence of geometric and thermal characteristics of the sensor and the environment on temperature measurement by direct contact has been studied by corroborating theoretical models with experimental measurements [27–31]. The chosen steady-state model assumes a medium of thermal conductivity λ and internal temperature T, limited by an adiabatic planar surface (except at the contact location) in non-perfect contact with a homogeneous, semi-infinite sensor rod in a circle of radius y (figure 10). The rod is perpendicular to the planar surface with thermal conductivity λ_e and exchanges thermal energy (positive or negative) with the ambient environment through its lateral surface by convection and radiation. The thermal exchanges between the medium and the thermometric sensor with the environment of temperature T_e can be represented by a heat transfer coefficient h_e. The temperature measured is then an average of the rod face at $x = 0$ to represent the average of a bead weld in a real thermocouple (non-intrinsic).

Under the condition $T > T_e$, the parasitic thermal transfer modifies the surface temperature due to thermal flux convergence toward the contact location:

$$T - T_p = r_m \Phi \tag{3}$$

where T_p is the perturbed surface temperature, Φ is the parasitic thermal flux, and r_m is termed the thermal macroconstriction resistance. Under the model assumptions for an isothermal contact circle, where the contact area and the size of the rod are equal, the macroconstriction resistance can be calculated as [27, 30]:

$$r_m = \frac{1}{4y\lambda}, \tag{4}$$

where 94% of the temperature disturbance $T - T_p$ occupies a circle of radius $10y$. The convergence effect is therefore prominent in materials with low thermal conductivity and/or small contact area.

The sensor does not measure the modified surface temperature but one that is further offset by a thermal contact resistance, r_c:

$$T_p - T_c = r_c \Phi, \tag{5}$$

where T_c is the temperature of the sensor face. It is challenging to experimentally or numerically determine the contact resistance value, since the effective surface contact area is much lower than the apparent contact area, due micro and macro surface texture. In addition, thermal contact resistance is affected by surface roughness, asperity slope, waviness, interstitial media, the pressure between contacting surfaces, the elastic properties, and the temperature of the interface. For this discussion, the value can be assimilated to equal to the thermal resistance of an interstitial interface media [30], e.g. grafoil, helium gas:

$$r_c = \frac{y_{\text{int}}}{\lambda_{\text{int}} \pi y^2}, \tag{6}$$

where y_{int} is the thickness of the thermal interface media, λ_{int} is its thermal conductivity, and y is the contact radius. The thermal contact resistance is therefore larger for sensors with a small contact area and inversely proportional to the thermal conductivity of the interface media.

Finally, the fin effect determines the thermal transfer between the face of the sensor at $x = 0$ and the external environment. The change in temperature between T_c and T_e is related to the parasitic thermal flux by the constant of proportionality r_e, the total thermal resistance between the sensor and the environment:

$$T_c - T_e = r_e \Phi. \tag{7}$$

The total thermal resistance can be determined by the following expression [27, 29]:

$$r_e = \frac{1}{\pi y_e \sqrt{2 h_e \lambda_e y_e}}, \tag{8}$$

where h_e is the heat exchange coefficient, λ_e is the thermal conductivity of the rod, and y_e is the radius of the rod (in this model $y = y_e$).

Combining equations (3), (5) and (7), the error in the measured temperature between T and T_c is given by:

$$\delta T = T - T_c = (r_c + r_m)\, \Phi, \tag{9}$$

with a heat flux:

$$\Phi = \frac{T - T_e}{r_c + r_m + r_e}. \tag{10}$$

Rearranging equation (10) and dividing equation (9) by $T - T_e$, the error can be expressed as:

$$\delta T = \frac{T - T_e}{1 + \frac{r_e}{r_c + r_m}}. \tag{11}$$

Therefore, the error in measuring temperature by contact will increase with the difference in temperature between the sample and the environment. This error can be reduced by increasing T_e so that $T \approx T_e$, for example, by using a thermally compensated temperature probe that maintains a low (or zero) heat flux through the sample–probe interface. However, practical implementation is challenging and may result in a positive heat flux into the sample. Additional mitigation strategies include reducing r_c and r_m while maintaining a large r_e. Even in the absence of a contact resistance, the ratio of the total thermal resistance and the macroconstriction resistance will dominate the error. The total thermal resistance can be increased by using small diameter and low thermal conductivity probe wires and supports with low emissivity, and by decreasing h through the use of radiation shielding and by evacuation of the sample chamber to high vacuum. These mitigation strategies are then central in the design phase of developing a tool to measure the Seebeck coefficient at high temperature.

We now apply the steady-state error model to elucidate the influence of contact geometry in the measurement of Seebeck coefficient. Low thermal conductivity is characteristic of thermoelectric materials, therefore macroconstriction resistance dominates the surface temperature measurement error. This error is larger for the 4-probe arrangement, since the contact area (i.e., y in the error model) is much smaller than the contact area for the 2-probe arrangement and is limited by the thermocouple bead size. In our apparatus, the 4-probe macroconstriction resistance is ≈10 times larger than r_m for the 2-probe, and the contact resistance is ≈125 times larger than r_c for the 2-probe, assuming the bead (diameter = 0.25 mm) is in complete contact with the surface. These errors can be mitigated by increasing the contact area to rod area ratio ($y \gg y_e$), for example, by using a trumpet shaped probe, where the contact end is flared. This increases y while maintaining a large r_e. The flare must also dilate in close proximity to the sample as not to modify the thermal response of the sensor with excess mass. Alternatively, a contact disc may be inserted to increase y and increase r_e by adding an additional r_m term between the disc and the sensor. Unfortunately, since the 4-probe contact geometry is off-axis to the direction of the thermal gradient, increasing the size of the contact area averages parallel isothermal planes and introduces additional error. In addition, this significantly increases the error in concurrent resistivity measurements wherein the thermocouple probe is used to measure the resistive voltage. Inserting the sensor directly within the sample may further reduce the macroconstriction and contact resistance by increasing the contact area, $s = 2\pi y L$, where L is the inserted sensor length. Here, the macroconstriction resistance is given by [29]:

$$r_m = \frac{1}{2\pi\lambda L} \log \frac{2y}{L} \quad \text{if } L \gg y. \tag{12}$$

The distribution and homogeneity of the interstitial contact material (e.g., colloidal graphite) may be quite complex and poses a challenge in calculating the actual resistance. In practice, this mounting technique is destructive to both the sample and the thermocouple.

In the 2-probe contact geometry, the thermocouple measures the temperature on the surface of a tungsten probe, which is in direct contact with the sample and therefore introduces two sets of interfacial thermal errors. However, the combination of these two error sets is likely to be much less than the single interface thermal error for the 4-probe arrangement by virtue of a design that optimally manages the errors. For example, in the 2-probe contact geometry, y can be as large as the sample cross sectional area while remaining in plane. This significantly reduces both the macroconstriction and contact resistance between the sample and the tungsten probe. The thermal interface between the thermocouple and the probe also has a very small convergence effect due to the high thermal conductivity of tungsten, even though y is small. Here, the thermal contact resistance dominates the error. Since the thermocouple is welded to the probe, a lower contact resistance can be achieved than by simply pressing the thermocouple bead directly onto the sample's surface. If welding is not possible, inserting the sensor within the probe may provide additional reduction in r_c. We note that the reduced macroconstriction and contact resistance conferred by the 2-probe contact geometry do not apply to situations wherein an isolated thermocouple bead is in direct contact with the end sample surface. Although the surface temperature is measured in plane, r_m and r_c are substantially increased by the small contact area of the bead.

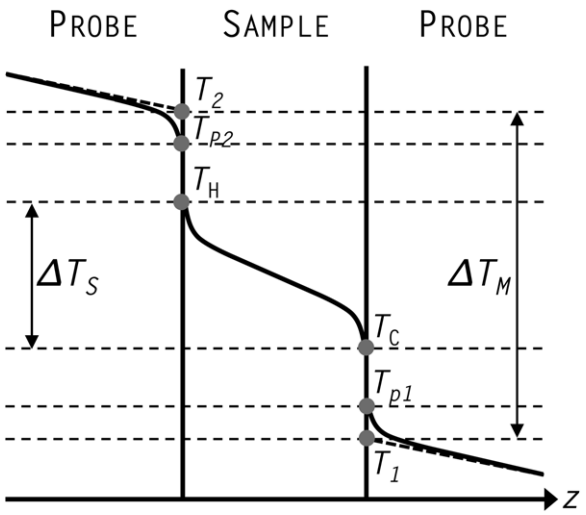

Figure 11. Diagram illustrating the error model applied to the 2-probe arrangement along the z-axis (along the sample thermal gradient). The actual temperature difference across the sample is given by $\Delta T_S = T_H - T_C$ and the measured temperature difference is given by $\Delta T_M = T_2 - T_1$.

Finally, the contact geometry determines the sign of error in the Seebeck coefficient. According to the error model, the temperature measured by surface contact is less than the temperature of the sample medium. Therefore, the 4-probe contact geometry underestimates the surface temperature measurement by δT_{4P}. This is further evidenced by the decrease in average sample temperatures for the 4-probe arrangement as compared to the 2-probe when measured under the identical stabilized thermal gradient. In addition, since there is a temperature difference between the two probes, T_2 and T_1, the hotter probe will always have a slightly greater error (equation (11)) than the cold probe, underestimating the temperature difference and thereby overestimating the Seebeck coefficient by δS_{4P}. The diagram in figure 11 illustrates a similar error model applied to the 2-probe arrangement but along the z-axis (along the sample thermal gradient). The actual temperature difference across the sample is given by $\Delta T_S = T_H - T_C$ and the measured temperature difference is given by $\Delta T_M = T_2 - T_1$ (ignoring for this diagram the contact between the probes and the thermometric sensors). Accordingly, the 2-probe arrangement, by nature of the thermophysical properties and geometry, will overestimate the temperature difference across the sample and thereby underestimate the Seebeck coefficient by δS_{2P}. This is supported by the observed pressure dependence of the Seebeck coefficient with a poor thermal contact (figure 2). Therefore, since $\delta T_{4P} \gg \delta T_{2P}$ and $\delta S_{4P} > 0 > \delta S_{2P}$, the absolute Seebeck coefficient measured in the 4-probe arrangement increases monotonically as linear function of the temperature difference between the sample and the external environment, when compared to the data measured in the 2-probe arrangement (figure 9). In addition, the data obtained under the 2-probe arrangement agree with data extrapolated from reliable literature data [32].

Conclusions

The measurement of surface temperature by contact is influenced by intrinsic thermal errors. Application of a sensor to the surface of the medium modifies the thermal interaction of the contacted surface with the environment, thereby inducing a parasitic thermal transfer between the sample and the sensor, and the sensor and the environment that perturbs the local temperature field. This error depends on the unique geometric and thermophysical characteristics of the system, the difference in temperature between the sample and the environment, and on the ratio of the total thermal resistance to the sum of the macroconstriction and contact resistance. For measurements of surface temperature in thermoelectric materials, the macroconstriction resistance will likely dominate the error. In addition, the macroconstriction and thermal contact resistances are larger in the 4-probe arrangement as compared to the 2-probe due to the smaller contact area. The contact area for the 4-probe arrangement cannot be sufficiently increased due to the off-axis geometry. The thermal contact resistance can be modified by using interstitial interface materials. Finally, the 4-probe contact geometry will tend to overestimate the absolute Seebeck coefficient, while the 2-probe will underestimate the value. In the search for higher efficiency thermoelectric materials, it may be prudent to implement the contact geometry that may modestly underestimate the Seebeck coefficient rather than one that may result in greater overestimation. Therefore, the contact geometry, dependent on the thermal interface, is the primary limit to high accuracy, while the measurement technique, under ideal conditions, has little influence on the measured Seebeck coefficient.

As a conservative measure, these results should not be taken as quantitatively indicative of all measurement apparatus or as reflective upon their data quality. These results do serve to illustrate the likely outcome of commonly adopted measurement practices currently employed among both commercially available and custom developed instrumentation. As such, the stated conclusions are expected to be qualitatively applicable to guide researchers in developing reasonable uncertainty limits.

References

[1] Wood C 1988 Materials for thermoelectric energy conversion *Rep. Prog. Phys.* **51** 459
[2] Mahan G D 1998 Good thermoelectrics *Solid State Physics* vol 51 ed H Ehrenreich and F Spaepen (New York: Academic) p 81
[3] Nolas G S, Sharp J and Goldsmid H J 2001 *Thermoelectrics: Basic Principles and New Materials Developments* (New York: Springer)
[4] Rowe D M (ed) 1995 *Thermoelectrics Handbook* (Boca Raton, FL: CRC Press)
[5] Kanatzidis M G, Mahanti S D and Hogan T P (ed) 2003 *Chemistry, Physics, and Materials Science of Thermoelectric Materials: Beyond Bismuth Telluride* (New York: Plenum)
[6] Martin J, Tritt T and Uher C 2010 High temperature Seebeck coefficient metrology *J. Appl. Phys.* **108** 121101
[7] Uher C 1996 TE materials *Nav. Res. Rev.* XLVIII 44

[8] Tritt T M 1997 Measurement and characterization techniques for thermoelectric materials *Thermoelectric Materials—New Directions and Approaches: Materials Research Society Symp. Proc.* vol 478 ed T M Tritt, M Kanazidis, G Mahan and H B Lyons (Pittsburgh, PA: MRS) p 25
[9] Tritt T M and Browning V 2001 *Recent Trends in Thermoelectric Materials Research I: Semiconductors and Semimetals* vol 69 ed T M Tritt (New York: Academic) pp 25–50
[10] Burkov T 2005 *Thermoelectrics Handbook: Macro to Nano* (Boca Raton, FL: CRC Press) p 22-1
[11] Tritt T M 2005 *Thermoelectrics Handbook: Macro to Nano* (Boca Raton, FL: CRC Press) p 23-1
[12] Magnus G 1851 *Pogg. Ann.* **83** 469
[13] Bowers R, Ure R W Jr, Bauerle J E and Cornish A J 1959 InAs and InSb as thermoelectric materials *J. Appl. Phys.* **30** 930
[14] Wood C, Zoltan D and Stapfer G 1985 Measurement of Seebeck coefficient using a light pulse *Rev. Sci. Instrum.* **56** 719
[15] Martin J 2012 Apparatus for the high temperature measurement of the Seebeck coefficient in thermoelectric materials *Rev. Sci. Instrum.* **83** 065101
[16] Bentley R 1998 *Theory and Practice of Thermoelectric Thermometry* (Singapore: Springer)
[17] Burns G W and Scroger M G 1989 *NIST Special Publication* 250–35
[18] Roberts R B, Righini F and Compton R C 1985 The absolute scale of thermoelectricity: III *Phil. Mag.* **52** 1147
[19] Burkov T, Heinrich A, Konstantinov P P, Nakama T and Yagasaki K 2001 Apparatus for the high temperature measurement of the Seebeck coefficient in thermoelectric materials *Meas. Sci. Technol.* **12** 264
[20] Runyan W R and Shaffer T J 1997 *Semiconductor Measurements and Instrumentation* 2nd edn (New York: McGraw-Hill)
[21] Streetman B G 1995 *Solid State Electronic Devices* (Englewood Cliffs, NJ: Prentice-Hall)
[22] Panagopoulos C, Fukami T and Aomine T 1993 The effects of gaseous helium and nitrogen on the thermopower measurements: a note of concern for the discrepancy of the results observed in high temperature superconductors *Japan. J. Appl. Phys.* **32** 4684
[23] Villaflor B and de Luna L H 1994 Comments on the effects of gaseous helium and nitrogen on the thermopower measurements: a note of concern for the discrepancy of the results observed in high temperature superconductors *Japan. J. Appl. Phys.* **33** 4051
[24] Lowhorn N D, Wong-Ng W, Lu Z-Q, Martin J, Green M L, Bonevich J E and Thomas E L 2011 Development of a Seebeck coefficient standard reference material *J. Mater. Res.* **26** 1983
[25] Martin J 2012 Error modeling of Seebeck coefficient measurements using finite-element analysis *J. Electron. Mater.* doi:10.1007/s11664-012-2212-5
[26] Nasby R D and Burgess E L 1972 Precipitation of dopants in silicon–germanium thermoelectric alloys *J. Appl. Phys.* **43** 2908
[27] Le Masson P and Dal M 2011 Analysis of errors in measurements and inversion *Thermal Measurements and Inverse Techniques* ed H R B Orlande, O Fudym, D Maillet and R M Cotta (Boca Raton, FL: CRC Press) pp 565–98
[28] Cassagne B, Kirsch G and Bardon J P 1980 Analyse theorique des erreurs liees aux transferts de chaleur parasites lors de la mesure d'une temperature de surface par contact *Int. J. Heat Mass Transfer* **23** 1207
[29] Garnier B, Lanzetta F, Lemasson P and Virgone J 2011 Lecture 5A: Measurements with contact in heat transfer: principles, implementation and pitfalls *Metti 5 Spring School (Roscoff, June 13–18)* pp 1–34
[30] Trombe A and Moreau J A 1995 Surface temperature measurement of semitransparent material by thermocouple in a real site experimental approach and simulation *Int. J. Heat Mass Transfer* **38** 2797
[31] Cassagne B and Leroy G 1982 Mesure de température de surface par contact en regime variable *Rev. Phys. Appl.* **17** 153
[32] Joshi G *et al* 2008 Enhanced thermoelectric figure-of-merit in nanostructured p-type silicon germanium bulk alloys *Nano Lett.* **8** 4670